Catal Lett (2008) 125:229–235
DOI 10.1007/s10562-008-9578-2

Spatially-Resolved Calorimetry: Using IR Thermography to Measure Temperature and Trapped NO_X Distributions on a NO_X Adsorber Catalyst

Khurram Aftab · Jasdeep Mandur · Hector Budman · Neal W. Currier · Aleksey Yezerets · William S. Epling

Received: 25 May 2008 / Accepted: 4 July 2008 / Published online: 23 July 2008

Abstract Spatial- and time-resolved temperature distributions over a $Pt/Ba/Al_2O_3$ model NO_X storage/reduction (NSR) catalyst were measured using infra-red thermography. The heat generated during regeneration was correlated to surface nitrate reduction, thereby revealing the concentration of surface nitrates at specific locations along the catalyst. The results demonstrate that there is more nitrate formation at upstream positions relative to downstream, or from front to back of the catalyst, with short trapping times. However, as more NO_X was trapped on the catalyst during longer trapping times, it was found that the largest amount of NO_X was trapped slightly downstream of the inlet, evolving to a local maximum in amount trapped. Applying infrared (IR) thermography to this system resulted in a spatially resolved calorimetry method via the correlation of temperature to the distribution of sorbed nitrate species along the catalyst.

Keywords NO_X storage · NO_X reduction · Lean NO_X traps · Infra-red thermography · Vehicle emissions · Spatially resolved calorimetry

1 Introduction

Engine manufacturers are under increasing pressure to increase fuel efficiency while at the same time reduce exhaust emissions. Lean-burn engines represent a potential solution for fuel economy improvement due to their increased efficiency relative to today's stoichiometric-burn gasoline engines. And in practice, reducing CO and hydrocarbon emissions, via oxidation to CO_2 and H_2O, in lean-burn engine exhaust is feasible due to the abundant O_2 in the exhaust. An inherent problem however is reducing NO_X to N_2 in that abundant O_2. The three-way catalytic converter has resulted in significant success over the years in reducing emissions from stoichiometric, gasoline-burning engines, but is ineffective toward NO_X reduction in lean-burn engine exhaust.

One recently developed solution for removing NO_X species in an oxidizing environment is NO_X storage/reduction (NSR) [1–3]. NO_X is reduced to N_2 via two consecutive phases of a cycle. In the first phase, typically termed lean or trapping, NO is catalytically oxidized to NO_2 and the NO_X (here defined as $NO + NO_2$) is stored on the catalyst, ultimately as a nitrite or nitrate. In the second step, typically called the rich or regeneration phase, the trapped NO_X is converted to N_2 via excess reductant, relative to O_2, present in the exhaust [4]. This first phase is normal engine operation and can last on the order of minutes. With time, the amount of NO_X trapped on the catalyst increases, and at some point, an unacceptable amount of NO_X may start slipping through the sample. At this point the catalyst must be "cleaned", or regenerated, while at the same time reducing the trapped NO_X species to N_2, and the second phase is triggered. Several approaches in making the reductant-rich mixture have been proposed, and include running the engine itself rich so that the combustion product exhaust gas is reductant-rich [5, 6], adding fuel to the exhaust stream [7], reforming fuel in the exhaust stream [8] or a combination of these. This phase of the cycle lasts on the order of a few seconds. Overall, the

K. Aftab · J. Mandur · H. Budman · W. S. Epling (✉)
Department of Chemical Engineering, University of Waterloo, Waterloo, ON, Canada N2L 3G1
e-mail: wepling@uwaterloo.ca

N. W. Currier · A. Yezerets
Cummins Inc., MC 50321, Columbus, IN 47201, USA

regeneration process must ensure that the catalyst is exposed to enough reductant to convert the trapped NO_X species to N_2, thereby cleaning or regenerating the catalyst for the next trapping phase, while at the same time accomplishing the ultimate goal of reducing NO_X to N_2.

To accomplish both the redox and acid–base chemistry reactions, NSR catalysts are typically composed of a precious metal component and an alkali or alkaline-earth component, both deposited on a high surface area support. The precious metal carries out NO oxidation to NO_2, can assist in the subsequent oxidation to nitrate, and catalyzes the reduction step converting nitrates to N_2. The alkali or alkaline earth acts as the NO_X storage component, forming the nitrite or nitrate species. Other components may be added, including oxygen-storage capacity components (OSC) and other precious metals for the redox steps [9–13].

Previous research has shown that gradients in surface chemistry and temperature on NSR catalysts form during operation [14, 15]. As part of the cycle involves sorption, there is an expected NO_X-species surface concentration gradient along the length of the catalyst bed, or monolith channel, and indeed such gradients have been inferred from gas species measurements inside a monolith channel during the trapping phase [14, 15]. Temperature gradients also form from reactions at the lean-to-rich or rich-to-lean phase transitions, between residual O_2 or reductant on the surface reacting with incoming reductant and O_2. Nitrate reduction, and OSC reduction and oxidation if an OSC component is present can also contribute to temperature gradients [16]. In general, for emissions catalyst applications, axial distributions of reaction, surface chemistry, and temperature all exist on or along the surface of the catalyst and resolving these leads to valid physical models of such systems.

The objectives of this study were to resolve temperature gradients formed during cyclic operation and then use these temperature profiles to determine the concentration of surface NO_X species along the surface of a model, Pt/Ba/Al_2O_3 NSR catalyst. The temperature changes were used as an indirect method of determining the surface NO_X species concentration gradients by monitoring the heat evolved during the regeneration phase, with the heat being associated with nitrate reduction.

2 Experimental

The catalyst sample used in these experiments was composed of Pt and Ba on an Al_2O_3 washcoat, all coated on a 400 cpsi cordierite monolith. The Pt load was 50 g/ft^3 of monolith, the Al_2O_3 was 1.6 g/in^3 and the Ba was 20 wt.% of the amount of Al_2O_3, as BaO. The catalyst size was 3″ by 3″ in width and length. The catalyst height was 3 cells, ~0.125″. This sample piece was therefore semi-two-dimensional, and the flat surface was analyzed using the thermography technique described below. A schematic example of such a sample is shown in Fig. 1.

Simulated exhaust gas was made using bottled gases provided by PraxAir. The individual gas flows to the reactor system were controlled and monitored using Bronkhorst mass flow controllers. The simulated exhaust gas composition for the lean phase was 5% H_2O, 5% CO_2, 10% O_2, 330 ppm NO and a balance of N_2. During the rich phase, the gas composition was 5% H_2O, 5% CO_2, 0% O_2, 0 ppm NO, 6% CO and a balance of N_2. The total flow was 14.08 l/min for both phases. The gas mixtures, excluding H_2O, were made in two separate manifolds separated by a fast-acting, four-way pneumatic switching valve. Therefore, one stream went to the reactor, and the other was simply vented. The speed for switching the valve between the flows was less than 1 s (advertised as <100 ms).

The mixture going to the reactor passed through a pre-heating section, which raised the temperature to >100 °C so that H_2O could be introduced. The complete gas mixture then passed through a second pre-heater to attain the targeted test temperature, which in this work was 300 °C. Once the desired temperature was reached, it was simply maintained by custom-made Watlow furnaces holding the reactor. The reactor was custom-manufactured from a rectangular block of stainless steel. A top-view schematic of the reactor is shown in Fig. 2. To accommodate a view of the catalyst surface for temperature measurements via IR thermography a hole was cut into the top of the reactor (dashed circle of Fig. 2) that was sealed with a sapphire window. The viewing area is 3″ by 3″, the same size as the sample used. A sapphire window was used rather than other types as it could survive the high temperatures and gas compositions used. The furnace holding the reactor was made significantly larger, especially in height, in an attempt to minimize heat loss through the window. The reactor was designed to deliver a square-wave of flow upon

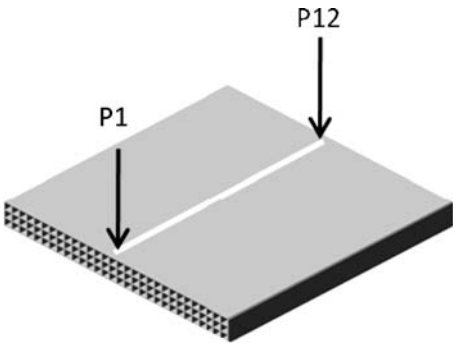

Fig. 1 Schematic of the sample shape used in this study. The dimensions are 3″ × 3″ × 0.125″. P1 and P12 indicate the positions of the end points of the twelve equidistant points used for data collection

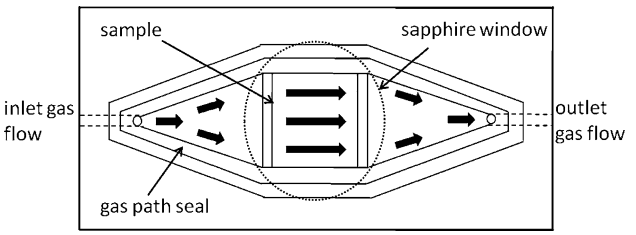

Fig. 2 Schematic of the reactor used in this study. The arrows represent gas flow direction. The dashed circle represents the placement of the sapphire window. The sample is indicated by the square in the center

reaching the sample, ultimately by keeping all angles in the flow path to the catalyst at a minimum. Evaluation of the temperature gradients that existed prior to reaction showed that there was a minimum in temperature at the sample center due to heat loss through the window, with the largest total difference across the catalyst in any direction being ~4 °C. Also, the reactor was built with four thermocouple fittings so that thermocouples could be set inside the reactor and channels of the monolith sample. During the experiments described, one was kept upstream of the sample, 2 inside different channels, and one on top of the sample, in view of the camera. When running inert gases through the reactor, the in-view thermocouple and camera readings always matched.

A FLIR Merlin series IR camera was used. The camera has a 320–256 focal plane array format for image resolution with an image collection frequency of 50 Hz. The area imaged was approximately 3 1/8″ by 3 1/8″. The camera has a sensitivity of 0.018 °C. The camera was placed over the reactor and recorded images of the catalyst surface through the sapphire glass window. Therma Cam Researcher™ software was used to transform the recorded color palette into temperature data. In this work, data are presented from 12 points, from the inlet to the outlet as described in Fig. 1, for presentation and analysis purposes. The 12 points are equidistant and fall on a line that is "radially" centered on the catalyst. In the discussion below, position 1 is the catalyst inlet and position 12 is the catalyst outlet, with the other 10 points spread between. Radial analysis is not presented, as this study focused on trends that developed down the length of a channel.

Experiments were run at 300 °C with NO as the NO_X source. Comparisons were made between experiments with increasing lean and rich phase times, specifically 30 and 90 s of lean phase, and 2, 4 and 8 s of rich phase. The surface temperature of the catalyst was continuously measured. In order to make analysis clearer, that data are plotted as a change in temperature rather than the absolute temperatures. The change in temperature should therefore reflect heat evolution due to reaction heat from any exothermic or endothermic reaction occurring on the surface. Numerous tests with this system have demonstrated that the rates of change in temperature measured by the thermocouple were noticeably slower than that of the camera, due to the thermal inertia of the thermocouple sheath. This also led to lower temperature intensities measured using the thermocouples, with these differences approaching 10% depending on the rate of the transient temperature change. In this study however, due to the lower temperature changes being measured, the differences were not significant.

An MKS MultiGas™ 2030 FTIR spectrometer was used to measure outlet gas compositions. The components measured were CO, CO_2, H_2O, NO, NO_2, NH_3 and N_2O, with data being obtained at ~2 Hz.

3 Results and Discussion

The NO_X slip data for the 90- and 30-s lean phase experiments obtained after steady cycle-to-cycle performance had been observed are plotted in Figs. 3 and 4. As shown, with increasing rich-phase time, the NO_X slip during trapping decreased for both lean times. These results suggest that even with 8 s of regeneration and 30 s of trapping time, residual nitrates might remain on the catalyst surface at the end of the regeneration phase since steady performance as a function of rich time was not achieved. Significant levels of CO, approaching 3–3.5% during 8-s regenerations and 0.4% during the 2-s regeneration, were observed, indicating that this was not due to a reductant limited scenario. Therefore, under the conditions of this test, the catalyst/conditions were not completely effective in inducing nitrate decomposition during the regeneration phase. In this case, such an inefficiency did not result in very poor performance, as 85–88% conversion was attained during the 30-s lean-phase experiments, and 67–75% conversions were obtained during the

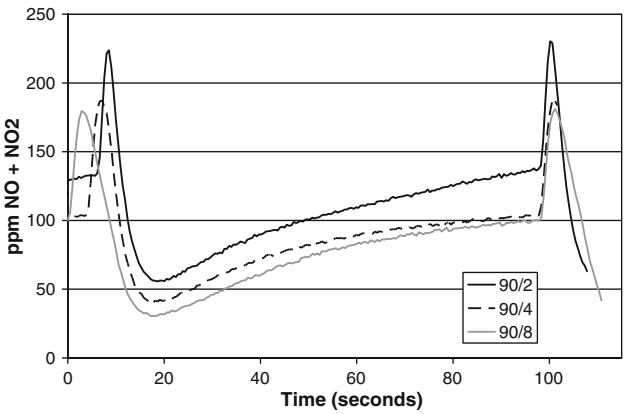

Fig. 3 NO_X ($NO + NO_2$) slip data as a function of time with 90-s lean phases and 2-, 4- or 8-s regeneration phases. Data were obtained at 300 °C. The plotted data were obtained after steady cycle-to-cycle performance was observed

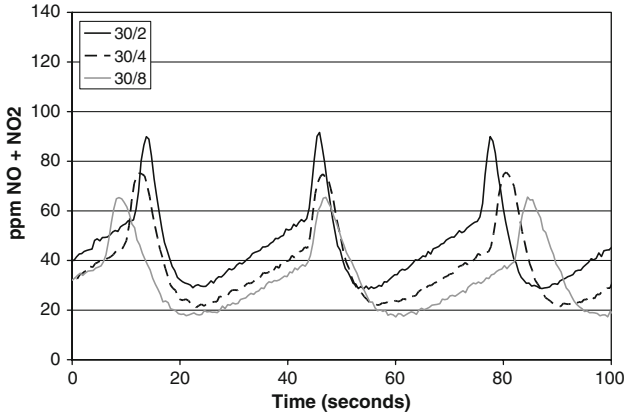

Fig. 4 NO_X (NO + NO_2) slip data as a function of time with 30-s lean phases and 2-, 4- or 8-s regeneration phases. Data were obtained at 300 °C. The plotted data were obtained after steady cycle-to-cycle performance was observed

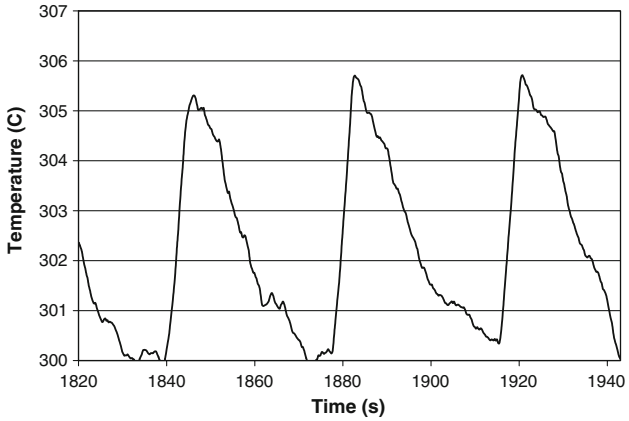

Fig. 5 Temperature measured via the IR camera at position 2 of 12 along the flow axis of the catalyst, while running at 300 °C with a 30-s lean phase and an 8-s rich phase

90-s lean-phase experiments. Also, as should be expected, with increasing lean-phase times, NO_X slip observed at the end of the trapping phase was higher for identical regeneration times. Furthermore, even when comparing NO_X slip after the onset of the trapping phase for both lean-time experiments, slip was lower during the first 30 s of the 30-s lean-phase time experiments in comparison to the first 30 s of the 90-s lean-phase time experiments. This again suggests incomplete regeneration for the 90-s lean time experiments.

Tests were performed in the absence of NO_X in the lean phase under otherwise identical conditions, and no temperature rise was observed, either with the camera or thermocouples, indicating that there were no measurable endothermic or exothermic reactions that could complicate interpretation when NO_X was added. Data obtained over 3 cycles from position 2, arbitrarily chosen, during a 30-s trapping, 8-s regeneration test, with NO_X, are shown in Fig. 5. The onset of the regeneration phase begins at approximately 1,838 s in this plot, and the temperature at position 2 begins rising after this time. At approximately 1,846 s, the temperature dropped, coincident with the switch back to the lean phase. The temperature increase is associated with the reduction of surface nitrates, which is an exothermic reaction process. We specify nitrates as at this test temperature, nitrite species are not typically observed, with nitrate species dominant [4]. These data also show that it takes many seconds for the temperature to drop back to the starting temperature, over 20 s in this experiment. As trapping efficiency is a function of temperature, this temperature rise during regeneration might influence the subsequent lean phase trapping performance as that heat is dissipated. Such an effect has been observed at higher operating temperatures with a commercial NSR catalyst [16]. In that study, a significant influence of heat generated during the regeneration phase on subsequent trapping was observed at test temperatures of 371 and 465 °C (with other tests performed at 200, 287, and 550 °C). NO_X slip increased with time after the onset of the trapping phase as expected, but then was observed to decrease after >20 s into the lean phase, which was coincident with the catalyst outlet temperature finally decreasing. This temperature decrease led to improved nitrate stability and an increase in trapping ability of the sample, thus the decrease in NO_X slip later in the trapping phase. With the sample used in the current study, this trend was not observed at 300 °C, likely due to the lower test temperature, as this trend was also not observed at 287 °C with the commercial sample either.

The maximum temperature rises observed at different positions on the sample during a cycle of the 30-s lean time experiments are shown in Fig. 6, and those for the 90-s lean time experiments are shown in Fig. 7. Data from position 1 have not been included; unfortunately having to

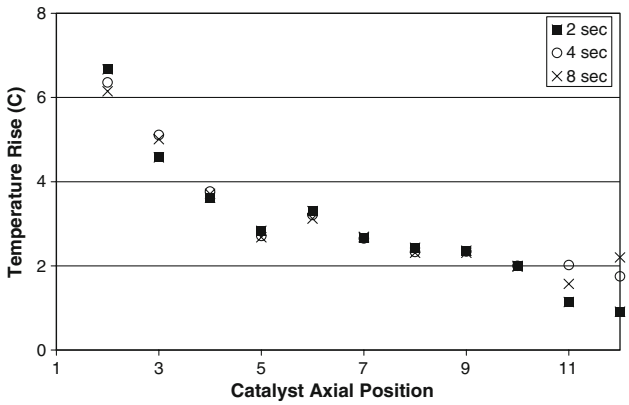

Fig. 6 Temperature differences measured as a function of axial position along the radial center of the sample, with 2-, 4- and 8-s regeneration phase times and a 30-s trapping time

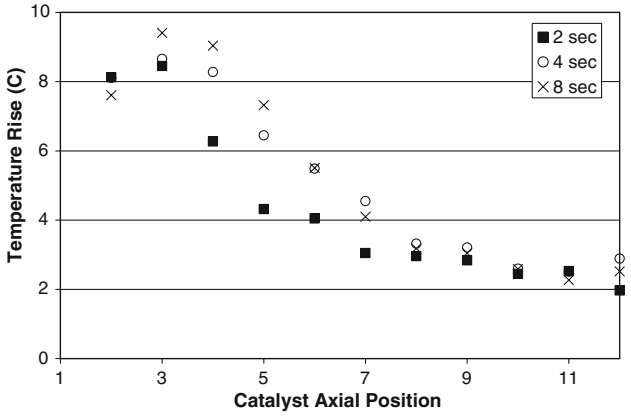

Fig. 7 Temperature differences measured as a function of axial position along the radial center of the sample, with 2-, 4- and 8-s regeneration phase times and a 90-s trapping time

be discarded due to the acquired raw data being confounded by reflection off the reactor walls. The outlet position was not influenced by reflection, simply due to the camera's position. As another note, the catalyst had a visual inhomogeneity in catalyst/washcoat character along the axial middle of the catalyst. This was observed for the entire monolith, and is likely due to preparation procedure. This inhomogeneity results in a different emissivity for that spot of sample, and obviously may also affect reactivity. These lead to a distinct change in trend at position 6–7 (the middle of the sample) as shown in Fig. 6. None-the-less, these do not detract from the overall trends and conclusions. As shown in Fig. 6, there was a small temperature rise at the catalyst inlet, on the order of 6–7 °C, which was observed during the regeneration portion of the cycle. There is no clear trend with respect to regeneration time, which is not surprising since the amounts trapped for the three experiments were not very different, 62.0, 65.6 and 67.4 μmoles, for the 2-, 4- and 8-s regeneration times, respectively. The largest temperature rise was observed at the very inlet, implying the largest amount of nitrate reduction occurs there, with decreasing amounts further downstream. This suggests a front-to-back decreasing surface concentration gradient as expected for a trapping bed. Since there was NO_X slip at the end of each trapping phase, some nitrate formation is expected along the entire length of catalyst. This is verified by the fact that at the outlet of the sample, there is still a measured temperature rise which indicates that there was some nitrate reduction even at the very outlet position. Furthermore, as noted above, CO was observed at the catalyst outlet during the regeneration, indicating that there were no limitations based on reductant absence. However, the data presented in Fig. 5 show that the temperature did not begin to decrease until the switch to the lean phase. It is therefore apparent that more reaction would have occurred if the regeneration time was extended, resulting in even higher temperature increases. Since CO was exiting the reactor, all positions were exposed to reactant for nitrate reduction, and therefore the relative heights of the temperature rise peaks are still indicative of the extent of nitrate reduction during the regeneration phase under the conditions of this test at that position. There are likely residual nitrates on the surface at the end of regeneration as discussed above, but the amounts correlated to the thermography data are the amounts being used in each cycle, once steady cycle-to-cycle performance was attained.

Increasing the lean time to 90 s, data shown in Fig. 7, resulted in an increase in the temperature rises observed relative to those observed with 30 s of trapping, indicating more nitrate reduction during regeneration. This suggests that more was trapped during the preceding lean phase as would be expected with a longer trapping time. Verifying this finding, the calculated amounts trapped for the three regeneration times were 150, 165 and 172 μmoles, for the 2-, 4- and 8-s regeneration times, respectively. The larger differences in amounts trapped as a function of regeneration time also led to differences in the observed temperature rises. In the catalyst region containing positions 3 through 6, the temperature rises associated with the 8-s regeneration are largest and those of the 2-s regeneration test are smallest. For example, at positions 4 and 5, the temperature differences for the 8-s regeneration were 9.0 and 7.3 °C, those for the 4-s regeneration were 8.3 and 6.5 °C, and those for the 2-s regeneration were 6.3 and 4.3 °C.

The temperature rise trend observed at the inlet positions is not consistent with those observed during the 30-s trapping tests. As shown in Fig. 7, the temperature rise increased between positions 2 and 3 for all three regeneration-time experiments. This indicates that there was not a smooth front-to-back saturation front as was observed with the 30-s trapping time experiments. For the 90-s lean time tests, beyond position 3, a steady decrease in temperature rise was observed, indicating that less NO_X was trapped at downstream positions, but only after position 3. Previous research has shown that NO_2 is trapped more readily than NO on NSR catalysts [17–24]. Furthermore, experimental data has been fit quite well using just NO_2 trapping and ignoring NO trapping [25], both suggesting that a likely explanation for the observed trend is limited NO oxidation leading to limited NO_2 for trapping. Predictive NO oxidation models do exist [26–29], as do models for NSR catalyst cycling [30–32], the latter study having also predicted a maximum in nitrate concentration slightly downstream of the inlet. Two of the trapping portion of the models were adapted for this study [30, 31]; adapted by inputting NO oxidation kinetics that include NO_2 inhibition [26], considering only NO_2 trapping kinetics with embedded diffusion resistance, and changing the catalyst details

used as inputs to match those of the sample used in this study. Specifically, the following reactions were used;

$$NO + {}^{1}/_{2}\ O_2 \rightarrow NO_2 (\text{reaction 1})$$

and

$$2NO_2 + {}^{1}/_{2}\ O_2 + BaCO_3 \rightarrow Ba(NO_3)_2 + CO_2 (\text{reaction 2}).$$

The rate expressions used are

$$r_1 = k_1 * C_{NO} * C_{O_2}^{0.5} - C_{NO_2}/K_{1eq}$$

$$r_2 = k_{2f} * \varphi_{NSC} * C_{NO_2} * C_{O_2}^{0.25} * \left(1 - \theta_{Ba(NO_3)2}\right) - k_{2b} * \varphi_{NSC} * C_{CO_2}^{0.5} * \theta_{Ba(NO_3)2}$$

with

$$k_1 = \left(7.5 * 10^5\right) * \exp(-40,000/R/T),$$

$$K_{eq} = \exp[(54,000 - 73.1 * T)/R/T],$$

$$k_{2f} = k_2/(1 + k_2 * L/D * r/r_{tot})$$

$$k_{2b} = (k_2/k_{eq})/(1 + k_2 * L/D * r/r_{tot})$$

where $k_2 = (1 * 10^{10}) * \exp(-75,000/R/T)$ and $k_{eq} = \exp[(114,000 - 125 * T)/R/T]$. The D (diffusivity) $= 6 \times 10^{-4}$ m^2/s, r_{tot} (radius of a Ba particle) $= 100$ nm, φ_{NSC} (total storage capacity) $= 90$ moles/m^3 of active washcoat and $L = r_{tot} - r$. The model was then used to predict the surface coverage of Ba species, under the further assumption that prior to trapping it is only Ba carbonate species on the surface and these are reacting to nitrates. The results are shown in Fig. 8. The prediction clearly shows that a minimum in carbonate coverage exists along the catalyst length for the 90-s trapping experiment, but one does not exist for the 30-s trapping experiment, lending confirmation to the data presented above. In summary, during the 30-s experiment, enough NO_2 was available for nitrate formation at the very upstream positions. During the 90-s experiment, the surface nitrate/gas phase NO_2 partial pressure equilibrium was approached at the very upstream positions. The extent of NO oxidation limited the amount of NO_2 in order to drive further nitrate formation. Further downstream, where more NO_2 was present simply due to more catalyst contact, more nitrate formation could occur due to the higher partial pressure.

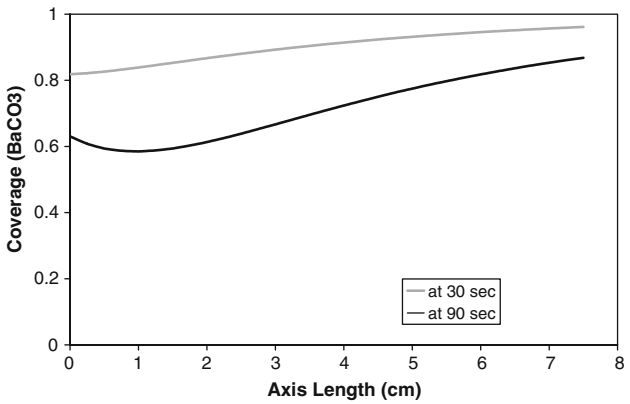

Fig. 8 Predicted $BaCO_3$ coverage as a function of catalyst length, for two different trapping times

4 Conclusions

The distribution of trapped NO_X along the length of a Pt/Ba/Al_2O_3 sample during NO_X storage and reduction cycles was indirectly measured using an infra-red camera. The temperature rise observed during regeneration, caused by exothermic nitrate reduction, was correlated to the amount of nitrate at that position formed during the previous trapping phase. The results demonstrate that for short trapping times, the concentration gradient of nitrates on the surface is monotonic, from front-to-back for high-to-low concentration. However, as the trapping time is increased, a maximum in amount trapped is observed, slightly downstream of the inlet position. This is attributed to higher levels of NO_2 at that position, with NO_2 building via NO oxidation at upstream positions. Results from an adapted model coincide with the experiment observations. Therefore, for NSR catalyst systems, not only can IR thermography provide accurate temperatures for kinetic model input, the data can also indirectly provide spatially-resolved nitrate species gradients along the catalyst.

Acknowledgements The authors would like to thank the Natural Sciences and Engineering Research Council of Canada and Cummins Inc. for funding of this work. We would also like to thank Johnson Matthey for supplying the samples used in this study.

References

1. Miyoshi N, Matsumoto S, Katoh K, Tanaka T, Harada J, Takahashi N, Yokota K, Sgiura M, Kasahara K, SAE Technical Paper Series 950809
2. Takahashi N, Shinjoh H, Iijima T, Suzuki T, Yamazaki K, Yokota K, Suzuki H, Miyoshi N, Matsumoto S, Tanizawa T, Tanaka T, Tateishi S, Kasahara K (1996) Catal Today 27:63
3. Brogan M, Brisley R, Walker A, Webster D, Boegner W, Fekete N, Kramer M, Krutzsch B, Voigtlander D, SAE Technical Paper Series 952490
4. Epling W, Campbell L, Yezerets A, Currier N, Parks J (2004) Catal Rev 46:163
5. Huff S, West B, Parks J, Swartz M, Green J, Graves R, SAE Technical Paper Series 2006-01-1416
6. West B, Huff S, Parks J, Lewis S, Choi JS, Partridge W, Storey J, SAE Technical Paper Series 2004-01-3023
7. Partridge W, Storey J, Smithwick R, Devault G, Cunningham M, Currier N, Yonushonis T, SAE Technical Paper Series 2000-01-2952
8. Kong Y, Crane S, Patel P, Taylor B, SAE Technical Paper Series 2004-01-0582

9. Mahzoul H, Brilhac J, Gilot P (1999) Appl Catal B Environ 20:47
10. Amberntsson A, Fridell E, Skoglundh M (2003) Appl Catal B Environ 46:429
11. Abdulhamid H, Fridell E, Skoglundh M (2006) Appl Catal B Environ 62:319
12. Theis J, Ura J, Goralski C, Jen H, Thanasiu E, Graves Y, Takami A, Yamada H, Miyoshi S, SAE Technical Paper Series 2003-01-1160
13. Ji Y, Toops T, Crocker M (2007) Catal Lett 119:257
14. Choi JS, Partridge WP, Daw CS (2005) Appl Catal A Gen 293:24
15. Choi JS, Partridge WP, Epling WS, Currier NW, Yonushonis TM (2006) Catal Today 114:102
16. Epling WS, Yezerets A, Currier NW (2006) Catal Lett 110:143
17. Salasc S, Skoglundh M, Fridell E (2002) Appl Catal B Environ 36:145
18. Mahzoul H, Brilhac JF, Gilot P (1999) Appl Catal B Environ 20:47
19. Prinetto F, Ghiotti G, Nova I, Lietti L, Tronconi E, Forzatti P (2001) J Phys Chem B 105:12732
20. Kobayashi T, Yamada T, Kayano K, SAE Technical Paper Series 970745
21. Fridell E, Persson H, Westerberg B, Olsson L, Skoglundh M (2000) Catal Lett 66:71
22. Kikuyama S, Matsukuma I, Kikuchi R, Sasaki K, Eguchi K (2002) Appl Catal A Gen 226:23
23. Laurent F, Pope C, Mahzoul H, Delfosse L, Gilot P (2003) Chem Eng Sci 58:1793
24. Schmitz P, Baird R (2002) J Phys Chem B 106:4172
25. Kromer BR, Cao L, Cumaranatunge L, Mulla SS, Ratts JL, Yezerets A, Currier NW, Ribeiro FH, Delgass N, Caruthers JM, accepted for publication in Catal Today
26. Mulla SS, Chen N, Cumaranatunge L, Blau GE, Zemlyanov DY, Delgass N, Epling WS, Ribeiro FH (2006) J Catal 241:389
27. Despres J, Elsener M, Koebel M, Kroecher O, Schnyder B, Wokaun A (2004) Appl Catal B Environ 50:73
28. Olsson L, Westerberg B, Persson H, Fridell E, Skoglundh M, Andersson B (1999) J Phys Chem B 103:10433
29. Crocoll M, Kureti S, Weisweiler W (2005) J Catal 229:480
30. Guthenke A, Chatterjee D, Weibel M, Walduber N, Koci P, Marek M, Kubicek M (2007) Chem Eng Sci 62:5357
31. Olsson L, Blint R, Fridell E (2005) Ind Eng Chem Res 44:3021
32. Schmeiber V, Tuttlies U, Eigenberger G (2007) Top Catal 42–43:77